

A SENSITIVE SEARCH FOR METHANE IN THE INFRARED SPECTRUM OF τ BOOTIS

Günter Wiedemann^{1,3}, Drake Deming², and Gordon Bjoraker^{2,3}

Received _____; accepted _____

arXiv:astro-ph/0007216v1 15 Jul 2000

¹European Southern Observatory, Karl-Schwarzschild-Str 2, Garching b. Muenchen, Germany

²Planetary Systems Branch, Code 693, Goddard Space Flight Center, Greenbelt MD 20771

³Visiting Astronomer at the Infrared Telescope Facility (IRTF), which is operated by the University of Hawaii, under contract with the National Aeronautics and Space Administration.

ABSTRACT

We have searched for a methane signature in the infrared spectrum of τ Bootis, produced by the planetary companion. The observations comprise 598 low-noise ($S/N \sim 100$), high resolution ($\lambda/\delta\lambda = 4 \times 10^4$) spectra near 3044 cm^{-1} , which we analyze by cross-correlating with a modeled planetary spectrum based on the work of Burrows and Sharp (1999), and Sudarsky et al. (2000). The 3σ random noise level of our analysis is $\sim 6 \times 10^{-5}$ stellar continuum flux units, and the confusion noise limit - measuring the resemblance of a cross-correlation feature to the spectrum of methane - is $\sim 2.5 \times 10^{-4}$.

We find a significant cross-correlation amplitude of $\sim 3.3 \times 10^{-4}$ continuum units at a velocity near that of the star. This is likely due to methane from a low-mass companion in a long-period orbit. Fischer, Butler and Marcy (2000) report a long-term velocity drift indicative of such a companion. But the system is known to be a visual binary with an eccentric orbit, and is rapidly approaching periastron. Whether the visual companion can account for our observations and the Fischer et al. velocity drift depends on knowing the orbit more precisely. The stability of planetary orbits in this system also depends crucially on the properties of the binary orbit.

A second cross-correlation feature, weaker and much more diffuse, has intensity amplitude $\sim 2 \times 10^{-4}$ continuum units and occurs at a velocity amplitude of $71 (\pm 10) \text{ km sec}^{-1}$, in agreement with the orbit claimed for the planet by Cameron et al. (1999). Like the first feature, it has passed several tests designed to reject systematic errors. We discuss the possibility that this second feature is due to the planet.

Subject headings: planetary systems - stars: individual (HR 5185) - stars: binary

(ADS 9025) - infrared: spectra

1. Introduction

The discovery of a planetary companion to 51 Pegasus (Mayor and Queloz 1995) has been followed by a flood of planet detections using the Doppler reflex technique (Marcy and Butler 1998, 2000). The so-called ‘hot Jupiters’ or ‘roasters’ (Sudarsky et al. 2000), are gas-giants (Charbonneau et al. 2000) in very short period orbits, where they both reflect and absorb significant amounts of stellar radiation. This opens the possibility of detecting their reflection of the visible stellar spectrum (Charbonneau et al. 1999, Cameron et al. 1999), or the infrared (IR) spectrum produced by the planets themselves.

The τ Boo planet is believed to be the hottest of the ‘roaster’ class, with $T \sim 1600$ Kelvins (Seager and Sasselov 1999, Sudarsky et al. 2000). Charbonneau et al. (1999) placed an upper limit on the reflected flux of 5×10^{-5} relative to the star. However, Cameron et al. (1999) claim a detection of reflected flux at the 2×10^{-4} level, at a planetary radial velocity amplitude of 74 km sec^{-1} . They mention the possibility that planetary molecular signatures might be detectable. This paper reports evidence for methane features in the τ Boo system, obtained using an IR spectral deconvolution technique.

2. Observations

Observations of τ Boo were made on UT 29 March - 3 April 1998 using the CSHELL spectrometer (Greene et al. 1993) on the 3-meter NASA IRTF on Mauna Kea. More than 1200 spectral frames were acquired under uniformly excellent observing conditions, and the actual integration time on τ Boo totaled to over 31 hours. Figure 1 shows the distribution of observations relative to the expected value of the planetary radial velocity during the run. The spectral region chosen was near 3044 cm^{-1} , where methane lines occur whose lower state energy will be significantly populated at the temperature of the τ Boo planet.

Numerous weak terrestrial absorptions due to ozone, methane, and water vapor also occur in this window. Figure 2 shows a high-resolution solar spectrum bracketing this region from the McMath-Pierce FTS (Delbouille et al. 1981); it reveals primarily terrestrial absorption. A weak solar iron line occurs near 3044.53 cm^{-1} (Livingston and Wallace 1991), but this line should be even weaker in the τ Boo spectrum. We convolved the FTS spectrum with a Gaussian whose FWHM was matched to the CSHELL resolution (0.076 cm^{-1}), and the resultant simulated CSHELL spectrum is also shown on Figure 2.

Observations of τ Boo were typically made as 90 second integrations at two positions on the slit, by nodding the telescope between ‘a’ and ‘b’ positions. The slit was oriented East-West, and the width was 0.5 arc-sec. Multiple reads of the 256x256 InSb array were made to reduce read noise to negligible levels. We typically sum four spectral frames in the order ‘abba’ with the sign of the ‘b’ frames made negative to subtract the background. Observations of a continuum lamp were made before, during, and after each night, and used to flat-field the spectra. A Krypton emission lamp was observed in various grating orders, and used to establish the wavelength calibration. Each of the 303 sums shows the star at both ‘a’ and ‘b’ slit positions. Extracting both spectra from each sum yields a total of 598 spectra, after a few low-quality spectra are rejected. A sample spectrum, extracted by the processing described in Sec. 4, is shown on Figure 2. All of the features visible in these spectra are due to terrestrial absorption. The observed τ Boo spectra are similar to the convolved FTS spectrum, the differences being attributable to humidity and altitude. The water line at 3042.39 cm^{-1} , for example, is much weaker in the τ Boo spectrum from Mauna Kea. Lunar spectra were also acquired with CSHELL to further characterize the terrestrial absorption spectrum.

3. Model Template Spectra

One form of spectral deconvolution is to cross-correlate (CC) the observed spectra with a modeled template spectrum (Deming et al. 2000). We computed a methane template from a model atmosphere, and also used it to simulate the planet in a set of ‘synthetic planet’ spectra (see Sec 4). The template spectrum was assumed to be independent of orbital phase. We used the temperature versus pressure profile for the ‘class IV’ atmosphere shown by Sudarsky et al. (2000, their Figure 1). Number fractions for methane at each pressure were calculated using the formulae given by Burrows and Sharp (1999), and solar abundances. A constant value was used for the continuous opacity, chosen to produce unit optical depth where the temperature equaled the effective temperature (1620K). The emergent flux spectrum was calculated, at sub-Doppler resolution, by a quadrature integration over emergent angle of intensity spectra. The line opacity profiles were taken as Voigt profiles, with depth-dependent Doppler broadening and damping. The damping was adopted to be 0.1 cm^{-1} per bar. The most current line data for methane were used (Brown 1999). A $T^{3/2}$ dependence was adopted for the rotational partition function (Robiette and Dang-Nhu 1979), and the vibrational partition function was calculated from the band centers listed by Brown et al. (1989). The emergent flux spectrum was convolved to the CSHELL spectral resolution.

Figure 3 shows the resultant methane spectrum; it is similar to the 51 Peg planet spectrum as modeled by Goukenleuque et al. (2000). Although most carbon will be in the form of CO at this temperature (Fegley and Lodders 1996, Burrows and Sharp 1999), the methane absorption in this spectral region remains sufficiently strong that the thermal modulation is limited by the overlapping profiles of saturated lines. In our template model, optical depth unity in the methane lines occurs in a pressure range of 0.01 to 0.1 bars, versus 10 bars for the continuum. A model with methane fractions reduced by

an order-of-magnitude was also computed (Figure 3), and it shows substantially more modulation than does the nominal model.

4. Data Processing

All of our data processing and analysis used procedures specifically written for this problem. The first stage in the data processing was to flat-field each frame, remove cosmic ray defects, and ‘hot pixels’. Flat-fielding consisted of dividing each frame by a continuum lamp frame. Cosmic rays produce very large deviations, and stellar spectra which were directly affected by them were discarded. Cosmic ray defects in the background were repaired in a manner similar to the hot pixels, which were replaced by an average of surrounding pixels. Following these corrections, the frames are summed in groups of four (‘abba’).

At the second stage of the data processing, we created a set of synthetic planetary spectra, by adding a Doppler-shifted and intensity-scaled version of the methane template spectrum to the flat-fielded data sums. The Doppler shifts were based on the Cameron et al. (1999) velocity amplitude, with the orbital ephemeris from Butler et al. (1997) and Marcy (1998). The intensity scale factor (ratio of planetary to stellar continuum fluxes) was 6.7×10^{-4} . This follows from a planetary radius of 1.8 Jupiter radii (Cameron et al. 1999) and 1620 Kelvin effective temperature (Sudarsky et al. 2000). The stellar temperature is near 6450 Kelvins (Perrin et al. 1977, Ford et al. 1999), with rotational $v \sin i = 15 \text{ km sec}^{-1}$ (Baliunas et al. 1997). We adopted a stellar radius of $2.0R_{\odot}$, which results from the Cameron et al. (1999) inclination (29°), combined with the assumption that the planetary orbit is locked to the stellar rotation. The synthetic and real spectra were processed and analyzed in parallel, using identical procedures.

Some spectra showed an intermittent fringing effect, not removed by the normal flat-fielding procedure. Fortunately, we were able to verify (by comparing continuum lamp scans made at different times) that the spacing of the fringes was constant. We therefore removed them using a Fourier notch filter; we applied exactly the same filter to the synthetic planet data. The slight tilt of the slit was corrected by spline-interpolating intensities in each row onto a standard wavenumber scale. We computed a wavenumber calibration for each row using six lines from Krypton lamp spectra taken on the first night, and applied zero-point corrections for subsequent nights using atmospheric lines. The wavenumber versus pixel relation used both a linear and quadratic term, as needed for optimal approximation of the grating equation. For each spectrum, we calculated the average spatial profile along the slit at both the ‘a’ and ‘b’ positions, and these profiles were fit to the intensities at each wavelength using linear least-squares. This is equivalent to the optimal extraction algorithm discussed by Horne (1986).

Terrestrial atmospheric lines were removed by scaling an atmospheric template spectrum in intensity, using linear least-squares. Our atmospheric template was constructed by averaging all of the continuum-removed ‘a’ and ‘b’ spectra, producing a template for each set. We also explored using lunar spectra to construct atmospheric templates, but the number of lunar spectra is far fewer, and we obtained the lowest CC noise levels by averaging the τ Boo spectra themselves. Because our observations cover a range of phase over nearly two orbital periods, planetary lines will not reinforce in this averaging, so the loss of planetary signal by fitting and subtracting this template will be minimal. Moreover, this and other processing effects are evaluated by the effect on the synthetic spectra, which are treated in an identical fashion.

After all processing, the resultant signal-to-noise (S/N) ratios (typically ~ 100) are close to the photon statistical limit, as shown for the collection of ‘b’ spectra on Figure 4

(the ‘a’ spectra are of equal quality). The remaining differences between the measured noise and the theoretical limit are due to variability of a few atmospheric lines relative to the template, as well as small intermittent imperfections in the array detector which are not completely removed by flat-fielding.

5. Cross-Correlation Analysis

Following Deming et al. (2000), we look for the presence of the planet from significant peaks in a CC function, $C(v_a, v_g)$, where v_a is the amplitude of the planetary orbital radial velocity, and v_g is the geocentric radial velocity of the center of mass (for our purpose, the stellar radial velocity). We derive CC error estimates using a Monte-Carlo technique (see Sec. 6). Although v_g is known (-19 km sec^{-1} for our observations), we treat it as a free parameter, to help distinguish between real and false signals. Similarly, we vary v_a over a range which includes negative amplitudes, out of phase with plausible planetary signals. We compute $C(v_a, v_g)$ as:

$$C(v_a, v_g) = N^{-1} \sum_{i=1}^N \left[\frac{\sum_{j=1}^M r_{ij} \tau_{ij} w_{ij}}{(\sum_{j=1}^M |\tau_{ij}|)(M^{-1} \sum_{j=1}^M w_{ij})} \right] \quad (1)$$

where r_{ij} is the residual intensity in τ Boo spectrum i at wavenumber ν_j , in units of the stellar continuum, after the processing described in Sec. 4. N is the number of spectra (598), and M is the number of wavelengths (256). The template values τ_{ij} are computed as:

$$\tau_{ij} = F'_\nu(\nu_j(1 - \frac{v_g + v_p^i}{c})) \quad (2)$$

where $F_\nu(\nu_j)$ is the planetary flux, in units of the stellar continuum flux, at wavenumber ν_j in the frame of the planet, and the prime indicates that the average value over the observed spectral interval has been subtracted. The $\frac{v_g + v_p}{c}$ factor shifts the wavenumber

scale to the observers frame. The planetary radial velocity v_p^i is computed as:

$$v_p^i = v_a \sin(2\pi(t_i - t_0)/P) \quad (3)$$

where $t_i - t_0$ is the time since 1998, March 29.58179 UT, and $P = 3.31267$ days (Butler et al., 1997, Marcy, 1998). The denominator in Eq. (1) provides a normalization for $C(v_a, v_g)$ such that its peak values are equal to the average amplitude of the planetary lines, in units of the stellar continuum flux. Positive CC values correspond to methane absorption spectra, and negative to emission. The w_{ij} are weights which allow for the variable quality of the data. We currently use:

$$w_{ij} = \sigma_i^{-2} \sigma_j^{-2} \quad (4)$$

where σ_i is the noise level of spectrum i and σ_j is the standard deviation of r_{ij} values at a given j .

6. Results

The number of photons detected over all wavelengths and summed over all 598 spectra is $\sim 2.2 \times 10^9$. Our best-case detection limit will approach the inverse square-root of this number, 2.1×10^{-5} . We replaced the real r_{ij} values with gaussian random noise whose amplitudes were equal to the photon noise level in each spectrum, and verified that the noise in $C(v_a, v_g)$ agrees with this limit. The noise levels achieved in the weighted real data produce $\sigma = 2.4 \times 10^{-5}$ in $C(v_a, v_g)$. The computed $C(v_a, v_g)$ values are shown as false-color images over a range of v_a and v_g in Figure 5. Two special locations marked on these images are the position of the center of mass, at $v_g = -19 \text{ km sec}^{-1}$, and the Cameron et al. (1999) claimed amplitude for the planet at $v_a = +74 \text{ km sec}^{-1}$. Figure 5a shows the results for the real data, 5b the synthetic data (which equals the real data plus a synthetic signal), 5c is the result when the data are replaced by gaussian random noise whose amplitude equals

the noise level in each spectrum, and 5d is the real data cross-correlated with a perturbed template (described below). To enhance the visibility of the planetary signature in Figure 5b, the synthetic signal is multiplied by 10.

The strongest peak on Figure 5a occurs at $v_g = -10 \text{ km sec}^{-1}$ and $v_a = -8 \text{ km sec}^{-1}$. Given that our spectral resolution is 7.5 km sec^{-1} , and template errors are also likely, this peak coincides with the stellar position to within the errors, and we refer to it as the ‘stellar peak’ (SP). Its amplitude is 3.3×10^{-4} , which is well above the random noise level. It is present when both the ‘a’ and ‘b’ spectra are analyzed separately. Since our template for terrestrial atmospheric removal uses an average of all the τ Boo data, this will tend to remove features near $v_a = 0$. However, the atmospheric template is used with a variable multiplier (depending on air mass), which will allow some fraction of features fixed in the stellar frame to survive the atmospheric corrections.

A second region of enhanced CC amplitude runs from the middle left to upper right, and passes close to the signal from the synthetic planet (5b) at the Cameron et al. (1999) amplitude of 74 km sec^{-1} . We refer to this region as the ‘planetary streak’ (PS). Its amplitude is $\sim 2 \times 10^{-4}$ in stellar continuum units, also well above the random noise. In our analysis, a feature at constant wavelength in the data will produce such slanted regions of enhanced CC amplitude. This occurs because a given wavelength is overlapped by a given template point over many pairs of values in (v_a, v_g) . Noise features can produce slanted patterns in either of two orthogonal directions. Planetary signals should be more concentrated at single points in the (v_a, v_g) plane, depending on the distribution of the observations in phase, as well as potential phase-dependent spectral variations. Since the majority of our observations (63%) happen to be made at negative planetary radial velocities (see Figure 1), using too negative a value for v_g is partially compensated by using a smaller v_a , and the observed CC amplitudes should slant from upper right to lower left,

qualitatively consistent with the observed slanting. Overexposed images of the synthetic planet CC amplitudes show this effect, but to a much smaller degree than the observed PS. Like the SP, the PS is present in both the ‘a’ and ‘b’ data.

We have subjected our results to numerous tests designed to identify false signals. Cool stellar spectra show vibrational OH lines in this region (Hinkle et al. 1995), but nothing resembling the SP/PS structure is produced by repeating our analysis using an OH template. A hot, optically thin planetary template, made by reducing the column density in the model atmosphere by several orders of magnitude, causes both the SP and PS to weaken greatly. We repeated the CC analysis using templates wherein the methane line wavelengths in the planetary model atmosphere calculation are given gaussian random perturbations with a standard deviation of 1.5 cm^{-1} . Computing 50 of these CC images, each representing ~ 500 CC values, we find that the standard deviation of the resultant ‘confusion noise’ is $\sigma = 8.2 \times 10^{-5}$. A randomly-selected example of such a perturbed CC analysis is shown on Figure 5d. Based on this test, the SP is a 4σ feature, and the PS is 2.4σ . We cannot envision how any error in our analysis could ‘know’ the real wavelengths of the methane lines in our template (Figure 3), so the appearance of the SP only with the correct template is credible evidence of a real methane signature.

Although the perturbed templates test indicates that the SP is a real methane signature, we must further establish that it is not produced by terrestrial methane, via an incomplete removal of the atmospheric spectrum. We computed several CC images where we deliberately under-corrected for terrestrial lines. These images show an increased noise level, but they do not show any SP/PS enhancement. We tried using the terrestrial spectrum (Figure 2) as an analysis template. This produces a feature similar to the SP but weaker (0.00026), and slightly closer to the terrestrial rest frame ($v_a = -5 \text{ km sec}^{-1}$). So at least a small portion of the terrestrial spectrum has survived our data processing.

However, the fact that the SP strengthens and shifts toward the stellar velocity when using the Figure 3 spectrum as a template indicates a significant contribution from methane in the τ Boo system.

7. Discussion

Based on the tests described above, we regard the SP as evidence for methane in τ Boo. The SP cannot be attributed to the planet in a 3.3-day orbit, because the SP velocity amplitude is near zero (within the errors). It cannot be due to the F7 star, which is much too hot to contain significant quantities of methane. Detailed interpretation of such a weak feature is necessarily problematic. Nevertheless, we tried templates characteristic of different temperatures, but found insufficient sensitivity to meaningfully constrain the temperature of the absorbing region(s).

We considered the possibility that this methane absorption might be circumstellar. But methane is not commonly seen in interstellar regions (Knacke et al. 1985), and is easily destroyed by stellar ultraviolet radiation (Mount and Moos 1978). Also, the SP is much weaker for optically thin templates, so it does not seem indicative of absorption by a thin homogenous medium (e.g., a tenuous circumstellar cloud). Instead, it is more consistent with methane occurring in an optically thick clump of column density $\sim 10^{21}$ cm^{-2} , with small filling factor relative to the star. This type of distribution suggests a compact object, such as a methane-dwarf. Can there be an undetected sub-stellar object in the τ Boo system? τ Boo was discovered to be a visual binary by Otto Struve in 1849, and Charbonneau (2000) has suggested that the M-dwarf companion may be contributing to our spectra. We here discuss the possibility that the M-dwarf, or a much cooler compact object, is producing the methane signal which we observe.

The M-dwarf companion is about 7 or 8 visual magnitudes fainter than the primary, and its spectral classification (M2) is at least 44 years old (Eggen 1956, attributes it to Kuiper). Two orbits for the system have been published, by Hale (1994) and Popovic and Pavlovic (1996). The orbital elements differ substantially. For example, Hale (1994) gives the eccentricity as 0.91 and the period as 2000 years, whereas Popovic and Pavlovic (1996) derive $e = 0.42$ and $P = 389$ years. Although the Hale orbit was published first, Hale made and utilized an observation of the system in 1991, which was apparently not known to Popovic and Pavlovic, who used observations prior to 1970. The orbits indicate that the position angle of the visual companion at the time of our observations was 30° (Hale orbit) or 37° (Popovic and Pavlovic orbit), with separation near 2.6 arc-sec in both cases. These values place the companion sufficiently off the CSHELL slit that no contribution to our observations would be possible.

However, there are additional relevant data for this system. Responding to our inquiry, Fischer, Butler and Marcy (2000) report that the primary star exhibits a long-term (~ 1990 to current) velocity drift of $-17 \text{ meters sec}^{-1} \text{ year}^{-1}$, requiring a companion in a long-period orbit. Can this reflex motion be caused by the M-dwarf? The Hale orbit predicts that the radial velocity of the M-dwarf will be changing by about $0.2 \text{ km sec}^{-1} \text{ year}^{-1}$ near periastron (in 2017). Assuming a mass ratio of ~ 10 , this would account for the drift reported by Fischer et al., but only if periastron occurs near 2000, instead of 2017. Interestingly, an earlier periastron would place the M-dwarf close to the slit during our observations. If the spectral type is significantly in error (which is plausible), and the companion is much cooler than M2, then it might show sufficient strength in the strong $3.3 \mu\text{m}$ methane band to account for the SP in our data. Also, if the Hale orbit is correct, the periastron distance of $\sim 22 \text{ a.u.}$ seems to preclude stable orbits for additional companions with periods of tens of years (Holman and Wiegert 1999). Alternately, if the Popovic and Pavlovic (1996) orbit is correct, the M-dwarf did not contribute to our observations, nor can it account for the

velocity drift observed by Fischer et al. (2000). So in this case another companion in the system would be indicated, and the periastron distance of ~ 66 a.u. for the M-dwarf might well permit stable orbits having periods of tens of years.

As for any signal so small (3 parts in 10^4), the reality of the SP should be confirmed by additional observations. Moreover, as discussed above, the interpretation of our data and the Fischer et al. (2000) velocity drift as indicative of additional sub-stellar companions in this system, depends crucially on precise knowledge of the orbit for the M-dwarf. Additional observations of the M-dwarf are badly needed, including separation, position angle, an updated spectral type, and observations of infrared colors.

The PS is also well above the random noise level of our analysis, but only marginally above the ‘confusion noise’ (2.4σ). Because the confusion noise is estimated by applying random perturbations to the wavelengths of the methane template lines (Sec. 6), it measures not only the reality of a cross-correlation feature, but also the degree to which a feature can be attributed to methane. Accepting the 2.4σ statistical significance for the moment, we consider the possibility that this methane signal is produced by the planet. The amplitude of the CC peak from the synthetic planet is 3×10^{-5} (the peak on Figure 5b has been amplified by 10, for clarity). So the PS (at 2×10^{-4}) is more than six times as large as the synthetic planet, which we have modeled to be consistent with the Cameron et al. (1999) planetary parameters. Since the Cameron et al. radius is already in modest excess of theoretical values (Guillot et al. 1996), it may seem that the PS amplitude is implausibly large. But the amplitude of our synthetic planet signal has been strongly reduced by the overlap of saturated lines (Figure 2). The chemical equilibrium abundance of methane (Burrows and Sharp 1999) will be competitive with CO only in the coolest regions of the planet’s atmosphere. If methane is convected to greater depths, then disequilibrium effects could result in a lower methane abundance (Griffith and Yelle 1999), and our synthetic

planet signal would increase. Also, we have assumed a stellar radius of $2R_{\odot}$, which follows from the Cameron et al. orbital inclination, the rotation data (Baliunas et al. 1997), and a synchronous assumption. A more conventional radius for the star (e.g., $1.4R_{\odot}$, Ford et al. 1999) will increase the size of the synthetic planet signal, since it is measured in stellar continuum flux units. We conclude that the amplitude of the PS is plausible for the planet.

At $v_g = -19 \text{ km sec}^{-1}$, the PS occurs at $v_a = +61 \text{ km sec}^{-1}$, whereas the Cameron et al. value is $v_a = +74 \text{ km sec}^{-1}$. If we entertain the possibility that the SP is displaced from the stellar position primarily by template error, then it is more appropriate to measure the difference in the Figure 5a ordinate between the SP and PS, which is $+81 \text{ km sec}^{-1}$. A reasonable estimate and error range for the PS position is to bracket these absolute and relative determinations, giving $+71 (\pm 10) \text{ km sec}^{-1}$. While this is consistent with the Cameron et al. value, the large spread of the PS into an extended streak seems inconsistent with a planetary origin. Nevertheless, it is possible that strong phase effects in the planetary spectrum could cause such large spreading in an analysis of this type. Observations with cryogenic cross-dispersed echelle spectrometers on 10-meter class telescopes (McLean et al. 1998) should be able to clarify the reality of this feature, and the role of spectral variation with phase, by providing very high S/N spectra over a much larger wavelength range.

8. Acknowledgments

We thank Adam Burrows for sending us methane cross-section data, Geoff Marcy for ephemeris data, and Linda Brown for providing the latest methane line parameters. We also thank Debra Fischer, Paul Butler and Geoff Marcy for communicating their results in advance of publication, and allowing us to quote them, and Bill Hartkopf for discussing the current status of the visual binary observations. We acknowledge extensive discussions on the data analysis and interpretation with Dennis Reuter and Don Jennings, and insightful

comments by Dave Charbonneau, Mike Mumma, Sara Seager, and Roger Yelle. This research was supported by the NASA Origins of Solar Systems program.

REFERENCES

- Baliunas, S. L., Henry, G. W., Donahue, R. A., Fekel, F. C., & Soon, W. H. 1997, *ApJ* (Letters), 474, L119
- Brown, L. R., Loete, M., & Hilico, J. C. 1989, *J. Mol. Spec.*, 133, 273
- Brown, L. R., 1999, private communication
- Burrows, A., & Sharp, C. M. 1999, *ApJ*, 512, 843
- Butler, R. P., Marcy, G. W., Williams, E., Hauser, H., & Shirts, P. 1997, *ApJ* (Letters), 474, L115
- Cameron, A. C., Horne, K., Penny, A., & James, D. 1999, *Nature* 402, 751
- Charbonneau, D., Noyes, R. W., Korzennik, S. G., Nisenson, P., Jha, S., Vogt, S. S., & Kibrick, R. I. 1999, *ApJ* (Letters), 522, L145
- Charbonneau, D. 2000, private communication.
- Charbonneau, D., Brown, T. M., Latham, D. W., & Mayor, M. 2000, *ApJ* (Letters), 529, L45
- Delbouille, L., Roland, G., Brault, J., & Testerman, L. 1981, *Photometric Atlas of the Solar Spectrum from 1850 to 10000 cm⁻¹*, Tucson: Kitt Peak National Observatory
- Deming, D., Wiedemann, G., & Bjoraker, G., 2000, in proceedings of the Giant Planets to Brown Dwarfs Workshop, eds. M. Marley & C. Griffith, Dordrecht: Kluwer, in press
- Eggen, O. J., 1956, *AJ* 61, 405
- Fegley, B. Jr., & Lodders, K. 1996, *ApJ* (Letters), 472, L37
- Fischer, D., Butler, R. P., & Marcy, G. M. 2000, private communication

- Ford, E. B., Rasio, F. A., & Sills, A. 1999, *ApJ*, 514, 411
- Goukenleuque, C., Bezar, B., Jouget, B., Lellouch, E., & Freedman, R. 2000, *Icarus* 143, 308
- Green, T. P., Tokunaga, A. T., Toomey, D. W., & Carr, J. S. 1993, *Proc. SPIE*, 1946, 313
- Griffith, C., & Yelle, C. A. 1999, *ApJ (Letters)*, 519, L85
- Guillot, T., Burrows, A., Hubbard, W. B., Lunine, J. I., & Saumon, D. 1996, *ApJ (Letters)*, 459, L35
- Hale, A., 1994, *AJ*, 107, 306
- Hinkle, K. H., Wallace, L. & Livingston, W. 1995, *Infrared Atlas of the Arcturus Spectrum, 0.9-5.3 Microns*, San Francisco: Astronomical Society of the Pacific.
- Holman, M. J., & Wiegert, P. A. 1999, *AJ*, 117, 621
- Horne, K. 1986, *PASP*, 98, 609
- Knacke R. F., Geballe, T. R., Knoll, K. S., & Tokunaga, A. T. 1985, *ApJ (Letters)* 298, L67
- Livingston, W., & Wallace, L. 1991, *An Atlas of the Solar Spectrum in the Infrared from 1850 to 9000 cm⁻¹ (1.1 to 5.4 μm)*, Tucson: National Solar Observatory, Technical Report 91-001.
- Marcy, G. W., 1998, private communication
- Marcy, G. W., & Butler, R. P. 1998, *ARA&A*, 36, 57
- Marcy, G. W., & Butler, R. P. 1998, *PASP*, 112, 137
- Mayor, M., & Queloz, D. 1995, *Nature*, 378, 355

McLean, I. S., & 14 co-authors, 1998, SPIE, 3354, 566M

Mount, G. H., & Moos, W. H. 1978, Ap.J. (Letters), 224, L35

Perrin, M. N., Nejlesen, P. M., Cayrel de Strobel, G., & Cayrel, R., 1977, A&A, 54, 779

Papovic, G. M., & Pavlovic, R. 1996, Bull. Astron. Belgrade 153, 57

Robiette, A. G., & Dang-Nhu, M. 1979, J. Quant. Spec. Radiat. Transf., 22, 499

Seager, S., & Sasselov, D. D. 1994, Ap.J. (Letters), 502, L157

Sudarsky, D., Burrows, A., & Pinto, P. 2000, ApJ, in press

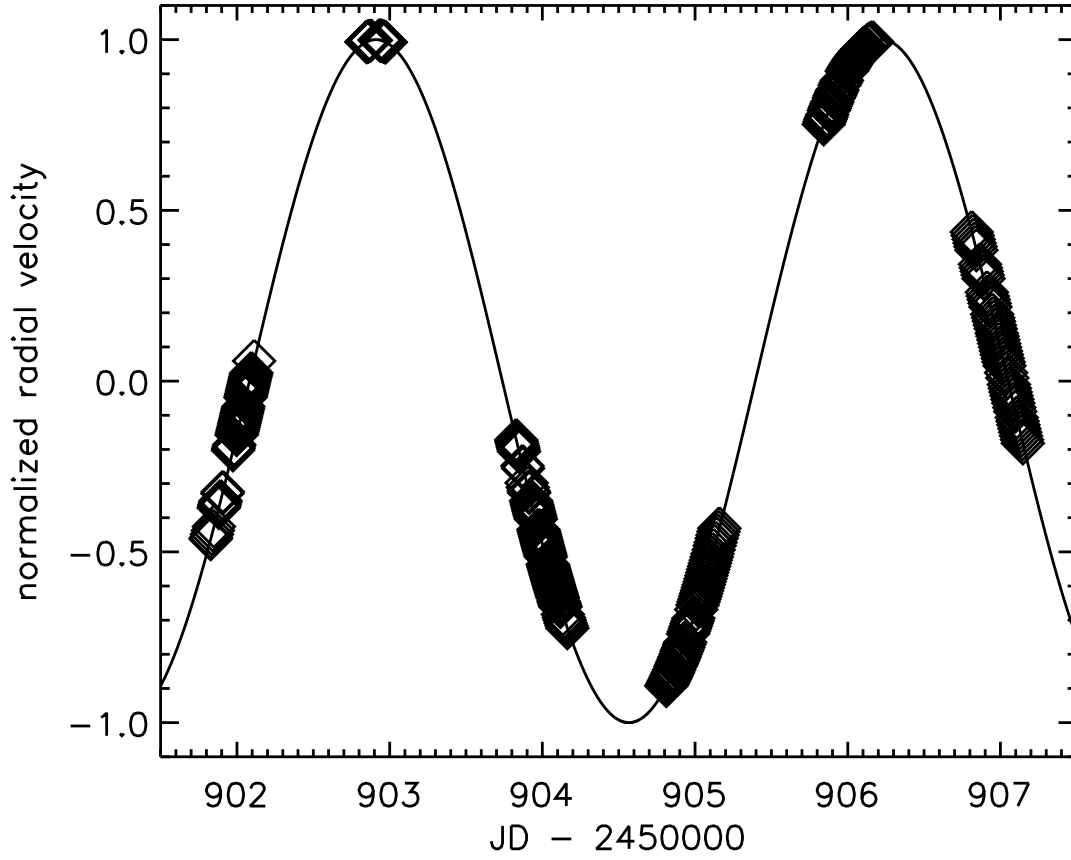


Fig. 1.— Distribution of the observations versus time. Phase is indicated by the planetary radial velocity, normalized to amplitude unity.

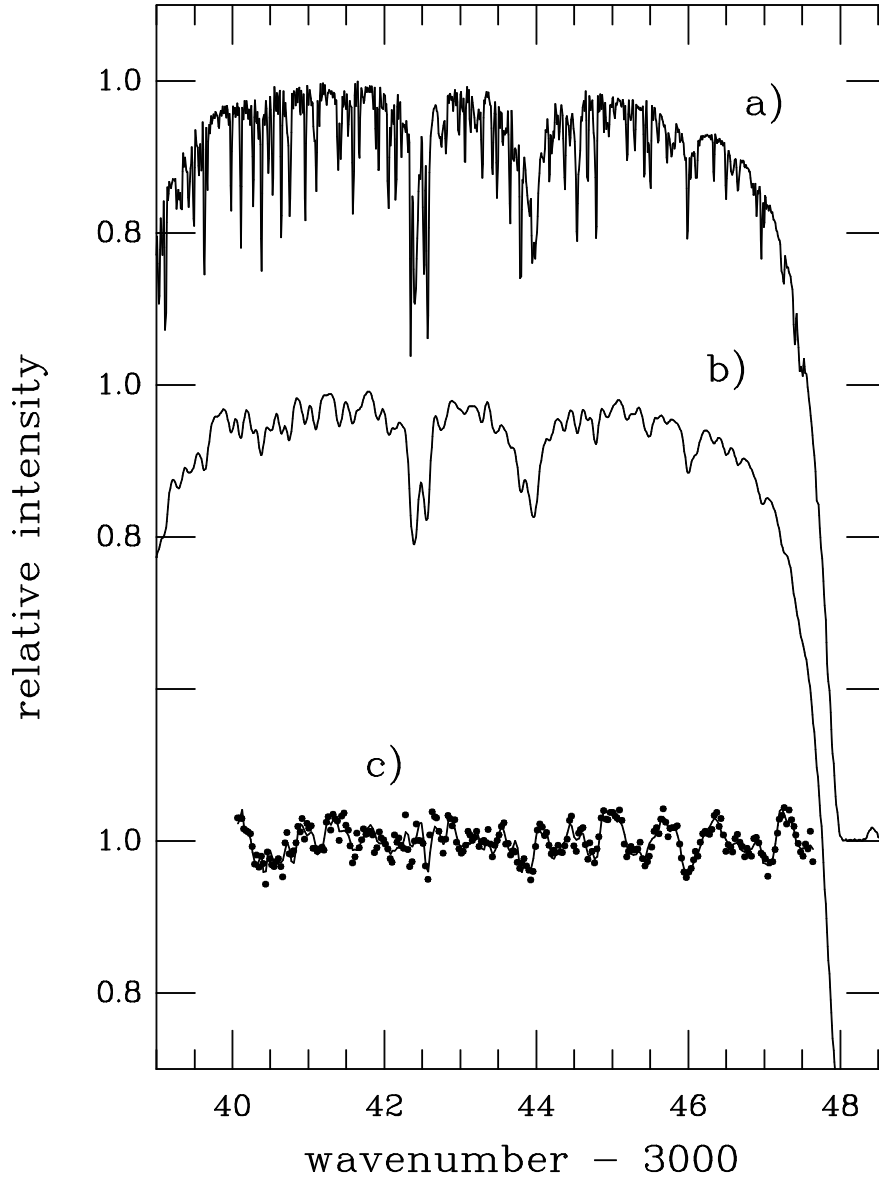


Fig. 2.— Sample spectra near 3044 cm^{-1} : a) high-resolution FTS solar spectrum from Kitt Peak, b) FTS solar spectrum convolved to CSHELL resolution, c) sample CSHELL spectrum (points) with the template fit (line).

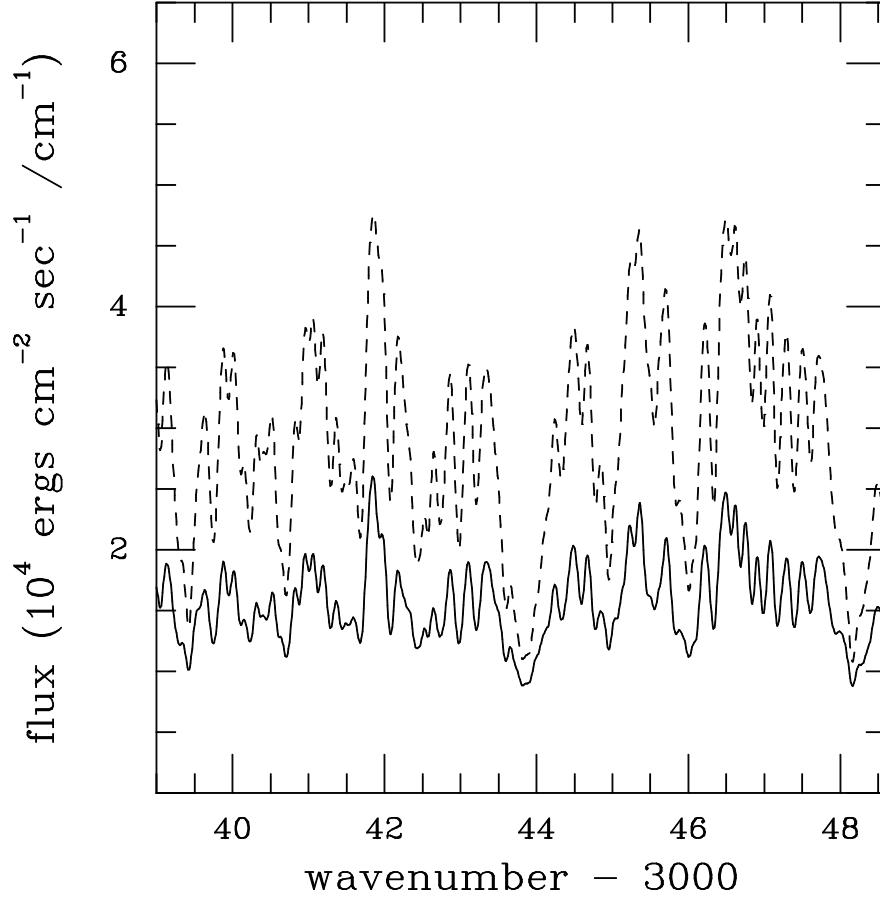


Fig. 3.— Modeled methane spectra near 3044 cm^{-1} . Solid line is the nominal τ Boo planet model, and the dashed line shows the effect of reducing the methane mixing ratio by a factor of 10. The continuum level is at 6.5×10^4 .

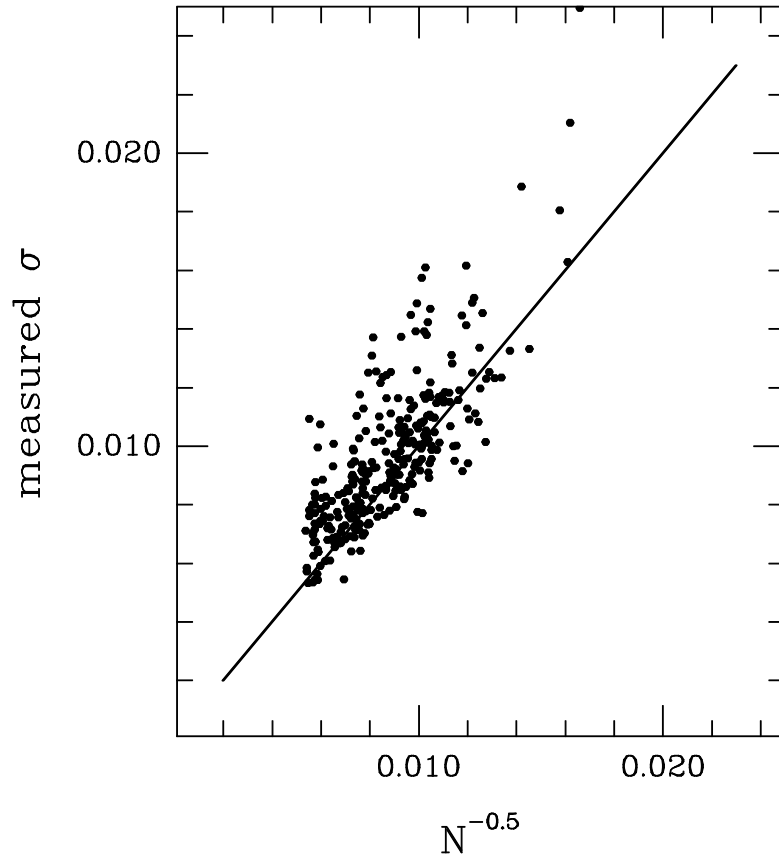


Fig. 4.— Measured noise level (standard deviation, in continuum units) versus the inverse root of the total number of photoelectrons detected per wavelength point. The line gives the photon statistical limit.

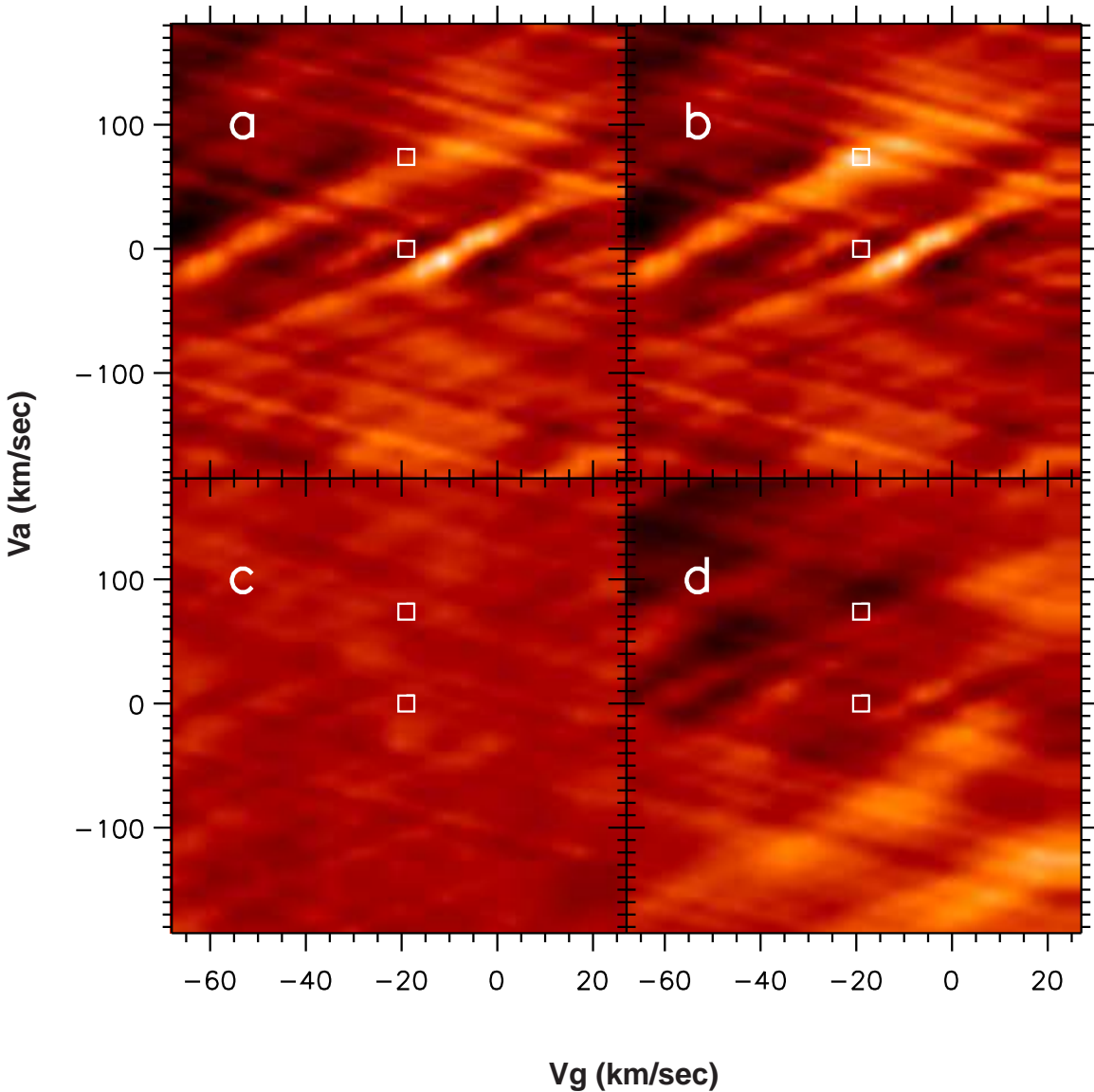


Figure 5. Cross-correlation amplitudes as false color images, versus assumed values of V_g and V_a . Each image is marked at the stellar velocity ($V_g = -19$, $V_a = 0$), and at the position of the planet ($V_g = -19$, $V_a = +74$, Cameron et al. 1999). The four cases are: a) the real data, b) the real data with the synthetic planet signal added, c) gaussian random noise with amplitude equal to the noise of the real data, and d) the real data analyzed with a template wherein the methane lines are scrambled in wavelength. The brightest portions of the images correspond to cross-correlation amplitudes of about 0.0003, and the darkest to amplitudes of about -0.0002.